THE JOURNAL OF PHYSICAL CHEMISTRY B

Article

pubs.acs.org/JPCB

Phase Behavior of Liquid Crystals with CO_2

Mariëtte de Groen, Thijs J. H. Vlugt, and Theo W. de Loos*

Engineering Thermodynamics, Process & Energy Department, Delft University of Technology, Leeghwaterstraat 44, 2628 CA Delft, The Netherlands

Supporting Information

ABSTRACT: Liquid crystals are being considered as novel process solvents for CO_2 capture. The solubility of CO_2 is higher in the isotropic phase than in the structured (e.g., nematic) phase. CO_2 can be captured in the isotropic phase, and regeneration of the solvent is achieved by cooling down the mixture a few degrees until a phase transition to the structured phase occurs. This CO_2 capture process has the potential to consume less energy than the conventional amine-based processes. To address the potential of liquid crystals to efficiently capture CO_2, experimentally obtained *P,T*-phase diagrams of five liquid crystals with 5 mass % CO_2 are reported. The liquid crystals used in this study are 4′-(pentyloxy)-4-biphenylcarbonitrile, 4′-pentyl-4-biphenylcarbonitrile, 4-ethyl-4′-propyl-bicyclohexyl, 4-propyl-4′-butyl-bicyclohexyl, and 4′-(octyloxy)-4-biphenylcarbonitrile. It is found that a weakly polar liquid crystal had a higher CO_2 solubility than apolar and more polar liquid crystals.

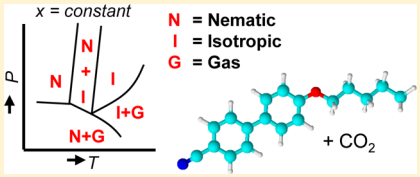

INTRODUCTION

Rod-like liquid crystals (LCs) are compounds having a structured liquid phase, called either nematic (N) or smectic phase (Sm) depending on the degree of ordering.[1] In the phase diagram, this structured liquid phase is located between the solid (S) and the usual isotropic liquid phase (I), shown in Figure 1. A liquid crystal can have only the smectic or nematic phase, or both types of phases. The first order phase transition between the structured and isotropic liquid can be controlled by varying the temperature. CO_2 is less soluble in the structured liquid than in the isotropic liquid.[2] Therefore, a liquid crystal may be used as a solubility switch:[2] CO_2 can be dissolved in the isotropic liquid phase and by cooling the isotropic mixture a few degrees, the structured phase is formed, and CO_2 is released again. The pressure is kept constant during this process. This CO_2 capture process has the potential to consume less energy than current processes.[2]

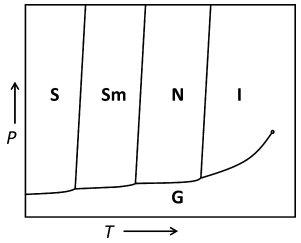

Figure 1. Schematic *P,T* diagram of a pure liquid crystal. S denotes a solid phase, Sm a smectic phase, N the nematic phase, I the isotropic phase, and G the gas phase.

For a CO_2 capture process using liquid crystals, the gas phase can be separated from the liquid phase at a three-phase equilibrium CIG: at this point, a structured phase (C), an isotropic phase (I), and a gas phase (G) coexist. C denotes a condensed phase: a solid phase, a smectic phase, or a nematic phase. Figure 2 shows a typical *P,T* and *T,x* projection of monovariant equilibria in systems of a low volatile component and a supercritical gas.[3] The *P,T* projection shows the pure component two-phase curves C ↔ I (CI), C ↔ G (CG), and I ↔ G (IG) and the pure component triple point CIG (△) of the low volatile component. The binary three-phase curve CIG

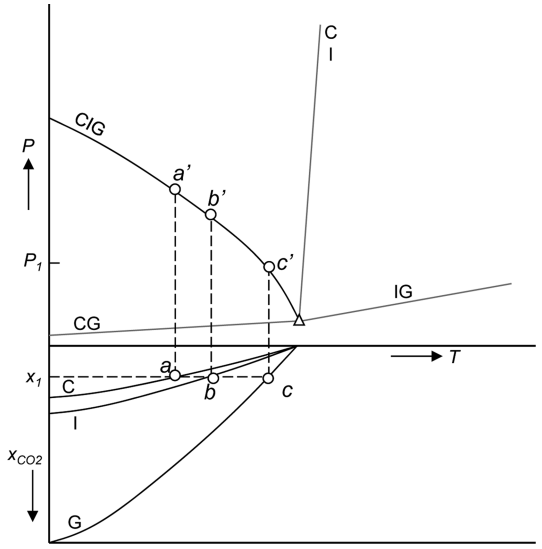

Figure 2. Schematic *P,T,x* projection of a liquid crystal with CO_2. C is either a nematic or a smectic phase, I is the isotropic phase, and G is the gas phase. △ is the triple point CIG of the pure LC. The labels a, b, c, a′, b′, and c′ are explained in the main text.

Received: April 10, 2012
Revised: June 25, 2012
Published: June 25, 2012

   dx.doi.org/10.1021/jp303426k | J. Phys. Chem. B 2012, 116, 9101−9106

starts in the triple point of the low volatile component, and in the case of CO_2 + LC systems, the derivative dP/dT is negative. This type of diagrams is well-known for systems of CO_2 and low-volatile organic compounds like CO_2 + naphthalene, and other asymmetric systems,[4] where C represents the solid phase of the low volatile component. In that case, the curve CIG is often referred to as the melting curve of the low volatile component under the pressure of a supercritical gas.[4] In the T,x projection of Figure 2, the composition of the three coexisting phases along the three-phase curve CIG is shown. The concentration of CO_2 in the condensed phase C is lower than that in the isotropic phase I. Note that if C is a solid phase then $x^{S}_{CO_2} \approx 0$. Except very close to the triple point temperature, the gas phase is almost pure CO_2. From Figure 2, a constant composition P,T diagram (isopleth) at CO_2 mole fraction x_1 (Figure 3) and an isobaric T,x diagram at P_1 (Figure 4) can be constructed. In these figures, C is either a nematic or a smectic phase.

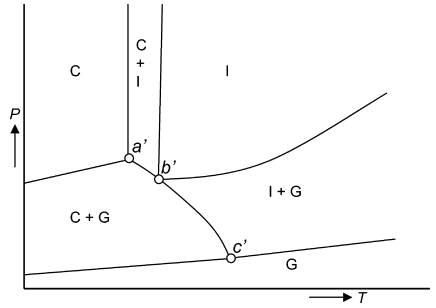

Figure 3. Schematic P,T diagram at constant x_1 (see Figure 1) of a liquid crystal with CO_2. C is either a nematic or a smectic phase, I is the isotropic phase, and G is the gas phase. The labels a, b, c, a′, b′, and c′ are explained in the main text.

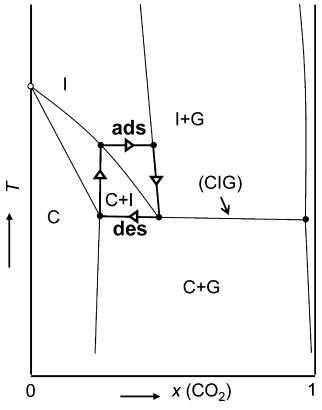

Figure 4. T,x diagram at constant pressure P_1 (see Figure 1) of a liquid crystal with CO_2. C is either a nematic or a smectic phase, I is the isotropic phase, and G is the gas phase. The boxed area connected by lines containing triangles represents the CO_2 adsorption (ads) and desorption (des) cycle as explained in the main text.

At concentration x_1 in the T,x projection of Figure 3, the three branches of the three-phase equilibrium curve are intersected at points a (C), b (I), and c (G). These points correspond to points a′, b′, and c′ in the P,T projection, respectively. In Figure 3, the three-phase curve CIG is only present between points a′ and c′ because of mass balance constraints. Figure 3 shows three two-phase regions (C + I, C + G, and I + G) and three one-phase regions (C, I, and G). The curves separating the I from the I + G region and the I + G region from the G region are the bubble-point curve and the dew-point curve of the I + G region, respectively. The curves separating the C region from the C + G region and the C + G region from the G region are the bubble-point curve and the dew-point curve of the C + G region, respectively.

In Figure 4, the T,x diagram at pressure P_1 is shown. At pressure P_1, upon increasing the temperature, first the three-phase equilibrium is found, represented in the figure with a horizontal line connecting the compositions of the C, I, and G phases. The other phase equilibria found are the phase transitions of the pure liquid crystal, C ↔ I and I ↔ G, respectively. At temperatures lower than the three-phase equilibrium temperature, the C + G area is found, and above this temperature, the two-phase regions C + I and I + G are present. In Figure 4, the absorption−desorption cycle is shown in a T,x diagram. The CO_2 desorption process takes place at the three-phase equilibrium CIG. The difference in solubility between the structured and isotropic phase determines the amount of CO_2 which can be captured during an absorption−desorption cycle. This depends on the width of the two-phase area C + I. The difference between the initial slopes ($x_{CO_2} \rightarrow 0$) of the C ↔ C + I and C + I ↔ I curves depends on the phase transition enthalpy and can be calculated using a modified van't Hoff law:[5]

$$\frac{dx^{C}_{CO_2}}{dT} - \frac{dx^{I}_{CO_2}}{dT} = \frac{\Delta_{tr}H}{RT_m^{\,2}} \quad (1)$$

Here, $\Delta_{tr}H$ is the phase transition enthalpy, which is positive for the structured to isotropic phase transition of the pure LC, $x^{C}_{CO_2}$ and $x^{I}_{CO_2}$ are the mole fractions of CO_2 in the structured and isotropic phase, respectively, T is the temperature, T_m is the melting temperature, and R is the gas constant. For capturing CO_2, nematic liquid crystals are most interesting because the viscosity of the nematic LCs is much lower than that of the smectic LCs. As values for $\Delta_{NI}H$, the phase transition temperature for the nematic to isotropic phase, which are published in the literature strongly scatter, eq 1 can only be used qualitatively as a measure of the width of the two-phase region for nematic liquid crystals. As an example, in Table 1, typical literature values for $\Delta_{NI}H$ are reported.

Table 1. Phase Transition Temperatures and Enthalpies for the Pure LCs Tested[a]

molecule	T_{SN} (K)	T_{SmN} (K)	T_{NI} (K)	$\Delta_{NI}H$ (kJ/mol)	T_{SmI} (K)
5CB	296[14]		308[15]	0.54[15]	
			308.35[16]	0.39[16]	
	296.9[d]		308.4[d]		
5OCB	320.5[b,15]		340.71[15]	0.42[15]	
	325.5[c,17]		340.55[16]	0.20[16]	
	326.8[c,d]		341.5[d]		
8OCB	326.01[15]	339.80[15]	352.58[15]	0.88[15]	
	327.7[e]		352.85[16]	0.40[16]	
			353.2[e]		
3,4-BCH					370[d]
2,3-BCH					341[d]

[a]S denotes the solid phase, Sm the smectic, N the nematic, and I the isotropic phase. [b]Solid phase S_1. [c]Solid phase S_2. [d]This work. [e]Provided by Prof. Picken.

dx.doi.org/10.1021/jp303426k | J. Phys. Chem. B 2012, 116, 9101−9106

Solubility measurements of CO_2 in liquid crystals using a gravimetric method[6−9] are described in the literature. Of the liquid crystals measured, PCH-5 has the highest mass based CO_2 solubility, followed by PCH8-CNS and MBBA.[8] A sharp increase in solubility between the isotropic and nematic phases was found.[2] With the gravimetric method, the presence of a two-phase region was found.[7]

In this paper, experimental *P,T* phase diagrams of binary mixtures of 5 mass % CO_2 with different liquid crystals with varying polarity and different alkyl chain lengths will be discussed. These phase diagrams will be used to discuss the influence of molecular structure and polarity on the solubility of CO_2 in liquid crystals.

EXPERIMENTAL METHODS

Materials. 4′-(Pentyloxy)-4-biphenylcarbonitrile, 99 mass % (5OCB), and 4′-pentyl-4-biphenylcarbonitrile, 99 mass % (5CB), were obtained from Alfa Aesar, 4-ethyl-4′-propyl-bicyclohexyl, >98 mass % (2,3-BCH), and 4-propyl-4′-butyl-bicyclohexyl, >98 mass % (3,4-BCH), were kindly supplied by Merck, 4′-(octyloxy)-4-biphenylcarbonitrile, >98 mass % (8OCB), was kindly supplied by Prof. Picken, Delft University of Technology, Delft, The Netherlands. Carbon dioxide was obtained from Linde Gas, with a purity of 4.5. All chemicals were used as received. In Table 1, the pure component properties of these liquid crystals are listed.

Phase Equilibria Measurements. A Cailletet apparatus was used to measure phase diagrams of mixtures of a liquid crystal and CO_2 with a known composition. The apparatus is described in detail elsewhere.[3] Liquid crystalline material was inserted as a solid or injected as a liquid in a glass sample tube, the Cailletet tube. The sample was weighed with a balance with an accuracy of 0.1 mg. The sample was degassed by repeated melting and freezing with liquid nitrogen. After the degassing was completed, 5 mass % of carbon dioxide was added while the mixture was frozen with liquid nitrogen. Mercury was used to seal the sample from the environment.

Phase transitions were observed visually by changing *T* at constant *P*, or *P* at constant *T*. The temperature was controlled using a Lauda RC 20 thermostatic bath, and was maintained constant within 0.02 K. The temperature was measured using a Pt100 resistance thermometer (ASL) with an estimated error of 0.01 K. The pressure was measured using a dead weight gauge (de Wit) with an accuracy of 0.005 MPa. The maximum error of (isotropic + gas) to isotropic (I + G ↔ I), (nematic + gas) to nematic (N + G ↔ N), and nematic + isotropic + gas (NIG) equilibria, measured at constant temperature, is ±0.005 MPa. The maximum error of the (solid + nematic) to nematic (S + N ↔ N), (solid + isotropic) to isotropic (S + I ↔ I), (smectic + nematic) to nematic (Sm + N ↔ N), (smectic + isotropic) to isotropic (Sm + I ↔ I), solid + nematic + gas (SNG), solid + isotropic + gas (SIG), smectic + nematic + gas (SmNG), and smectic + isotropic + gas (SmIG) equilibria measured at constant pressure is ±0.03 K. The (nematic + isotropic) to isotropic (N + I ↔ I) and the nematic to (nematic + isotropic) (N ↔ N + I) transitions have been measured within an accuracy of 0.01 K, unless otherwise stated. In the case of equilibria involving a smectic phase, only transitions in which the smectic phase disappears could be measured, because of the high viscosity of this phase.

RESULTS AND DISCUSSION

The liquid crystals tested can be divided into three different classes: apolar liquid crystals, polar liquid crystals, and weakly polar liquid crystals. The measured data points are available in the Supporting Information. The apolar liquid crystals, 2,3-BCH and 3,4-BCH, have a crystal to smectic phase transition and at a higher temperature a smectic to isotropic phase transition. Phase equilibria measured for these systems are the three-phase curve SmIG, the bubble-point curve I + G ↔ I, and the curve separating the two-phase region (Sm + I) and the one-phase area I. The phase diagrams of 2,3-BCH and 3,4-BCH with 5 mass % CO_2 are provided in Figures 5 and 6. The addition of CO_2 causes melting point depression: the smectic to isotropic phase transition temperature is shifted to lower temperatures. This is in agreement with eq 1. For comparison,

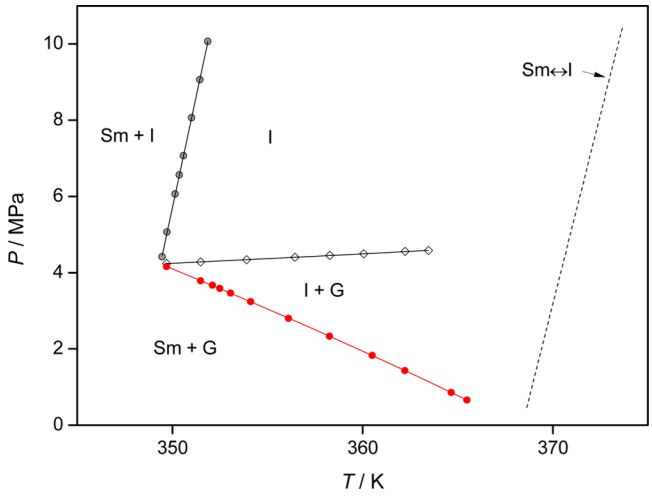

Figure 5. *P,T* diagram of propyl-butyl bicyclohexyl + 5 mass % CO_2. Description of symbols used: (gray ●) Sm + I ↔ I, (◇) I + G ↔ I, (red ●) Sm + I + G. The three-phase curve is identified with a red line and symbols and has notation between parentheses. The dashed curve is the Sm ↔ I phase transition of the pure LC.

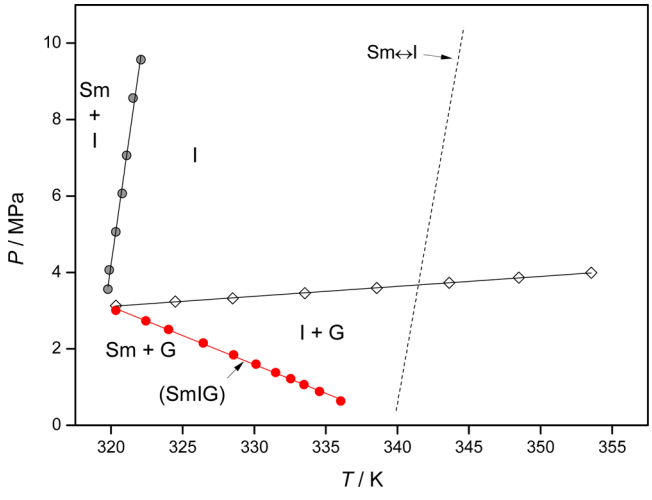

Figure 6. *P,T* diagram of ethyl-propyl bicyclohexyl + 5 mass % CO_2. Description of symbols used: (gray ●) Sm + I ↔ I, (◇) I + G ↔ I, (red ●) Sm + I + G. The three-phase curve is identified with a red line and symbols and has notation between parentheses. The dashed curve is the Sm ↔ I phase transition of the pure LC.

dx.doi.org/10.1021/jp303426k | J. Phys. Chem. B 2012, 116, 9101−9106

the pure component Sm ↔ I curve is shown in the figures as a dashed curve. The I + G ↔ I curve of 3,4-BCH is found at a higher pressure than the I + G ↔ I curve of 2,3-BCH. Figure 5 and 6 correspond to the higher temperature part of Figure 3 for C is defined as being a smectic phase.

The pure liquid crystal 8OCB shows a different behavior: at atmospheric pressure and 328 K, it has a phase transition from solid to smectic, at 340 K from the smectic to the nematic phase, and at 353 K from the nematic to the isotropic phase. The phase diagram of this liquid crystal with 5 mass % CO_2 is presented in Figure 7. Bubble points of 8OCB + 5 mass % CO_2

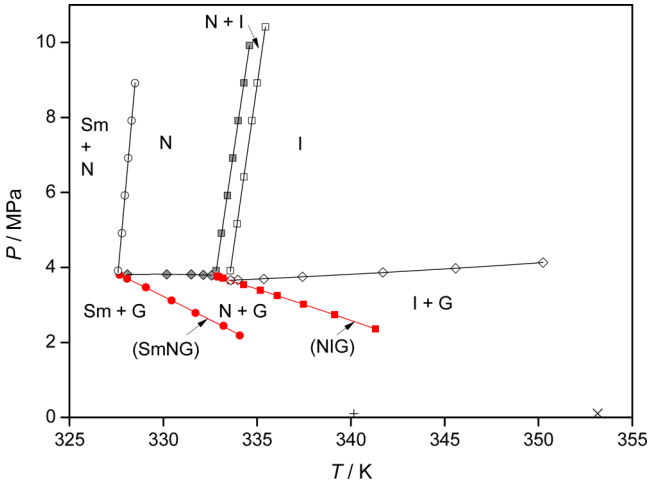

Figure 7. *P,T* diagram of octyloxy cyanobiphenyl + 5 mass % CO_2. Description of symbols used: (○) Sm + N ↔ N, (gray ■) N ↔ N + I, (□) N + I ↔ I, (gray ◆) N + G ↔ N, (◇) I + G ↔ I, (red ●) Sm + N + G, (red ■) N + I + G, (+) Sm ↔ N for the pure LC at 1 bar, (×) N ↔ I for the pure LC at 1 bar. Three-phase curves are identified with red lines and symbols and have notations between parentheses.

were measured for both the nematic and the isotropic phase. Compared to the end point of the bubble-point curve of the nematic phase, the bubble-point curve of the isotropic phase starts at a lower pressure. The temperature of the smectic to nematic and the nematic to isotropic phase transition is shifted to lower temperatures, and due to the binary nature of the system, the phase transition became a trajectory instead of a sharp transition. The width of the two-phase area N + I is 0.8 K, and the isotropic phase starts to form at 332.8 K and 3.9 MPa. Two three-phase curves were measured for this system: the SmNG curve and the NIG curve. The SmNG curve is measured from the intersection of the bubble-point curve and the Sm + N ↔ N phase transition line, and the NIG curve starts at the intersection of the bubble-point curve and the N ↔ N + I phase transition line.

The phase diagram of 5OCB with 5 mass % CO_2 is shown in Figure 8.[10] For 5OCB, two solid phases were found, S_1 and S_2. Pure 5OCB has a N ↔ I transition at 341 K, a S_1 ↔ N transition at 324 K, and a metastable S_2 ↔ N transition at 317 K. Figure 8 shows the phase behavior of 5OCB with 5 mass % CO_2. When CO_2 is added to the liquid crystal, the S_2 phase becomes more stable than the S_1 phase. Therefore, a quadruple point S_1S_2NG was found at 314.9 K, 2.49 MPa. At this point, four three-phase curves should intersect: the S_1NG, S_2NG, S_1S_2N, and S_1S_2G curves. The last two mentioned three-phase curves could not be detected with the used experimental method, as it would require the detection of solid−solid

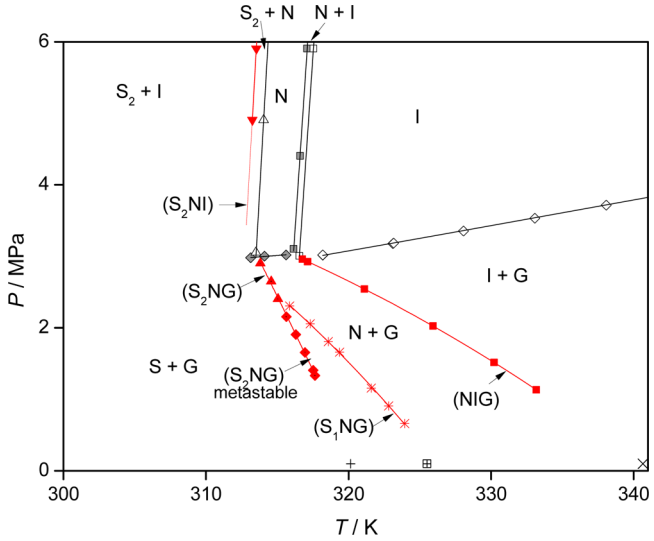

Figure 8. Part of the *P,T* diagram of pentyloxy cyanobiphenyl + 5 mass % CO_2. Description of symbols used: (red ▼) S_2 + N + I, (△) S_2 + N ↔ N, (gray ■) N ↔ N + I, (□) N + I ↔ I, (gray ◆) N + G ↔ N, (◇) I + G ↔ I, (red ▲) S_2 + N + G, (red ◆) metastable S_2 + N + G, (red ∗) S_1 + N + G, (red ■) N + I + G, + S_2 ↔ N for the pure LC at 1 bar, (⊞) S_1 ↔ N for the pure LC at 1 bar, (×) N ↔ I for the pure LC at 1 bar. Three-phase curves are identified with red lines and symbols and have notations between parentheses.

transitions. At temperatures lower than this quadruple point, S_2 is most stable and the three-phase equilibrium line S_2NG is found. However, as the S_1 ↔ S_2 phase transition does not occur instantaneously, part of this line is measured in the metastable region. As the melting point depression for the nematic phase is larger than that for the solid phase, an intersection of the S_2NI and S_2NG lines is found at 312.8 K, 3.32 MPa. This intersection is the quadruple point S_2NIG, where the three-phase equilibrium curves S_2NG, NIG, S_2NI, and S_2IG intersect. At temperatures lower than the quadruple point, the nematic phase becomes metastable. The boundary between the S_2 + I and S_2 + N two-phase regions is the S_2NI three-phase line. At temperatures below this quadruple point, the nematic phase is not stable anymore.

Pure 5CB has a crystal ↔ nematic and a nematic ↔ isotropic phase transition. The phase diagram of this liquid crystal with 5 mass % CO_2 is shown in Figure 9. As the nematic region of the pure component is smaller than that of the other liquid crystals tested, the nematic phase is less stable than the solid phase and the quadruple point SNIG is found at around 288 K, 1.4 MPa. Here the three-phase curves NIG, SNG, SIG, and SNI should intersect, but the SNI phase transition could not be measured at this concentration. When the solid is not crystallizing, the metastable part of the phase diagram is found, with the nematic to isotropic phase transition. The metastable part of the diagram is shown in Figure 10.

The solubility of CO_2 is influenced by the polarity of the liquid crystal. As illustrated in Figure 11, the apolar liquid crystals have the lowest mass based solubility and 5CB the highest solubility. The solubility of CO_2 in the case of 5CB is higher than that in the case of 5OCB, but in the literature, ether groups are considered to increase the solubility of CO_2.[11] A possible explanation for this behavior is a distorted quadrupolar moment of the benzene ring, leading to decreased affinity for CO_2. Benzene rings have a quadrupolar moment, and ab initio computations have shown that CO_2 forms transient hetero-

dx.doi.org/10.1021/jp303426k | J. Phys. Chem. B 2012, 116, 9101−9106

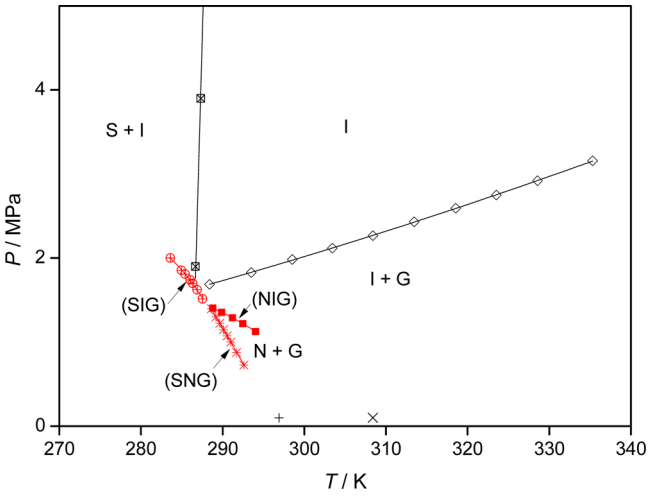

Figure 9. Part of the *P,T* diagram of pentyl cyanobiphenyl + 5 mass % CO_2. Description of symbols used: (□ with × in middle) S + I ↔ I, (red ⊕) S + I + G, (◇) I + G ↔ I, (red ∗) S + N + G, (red ■) N + I + G, (+) S ↔ N for the pure LC at 1 bar, (×) N ↔ I for the pure LC at 1 bar. Three-phase curves are identified with red lines and symbols and have notations between parentheses.

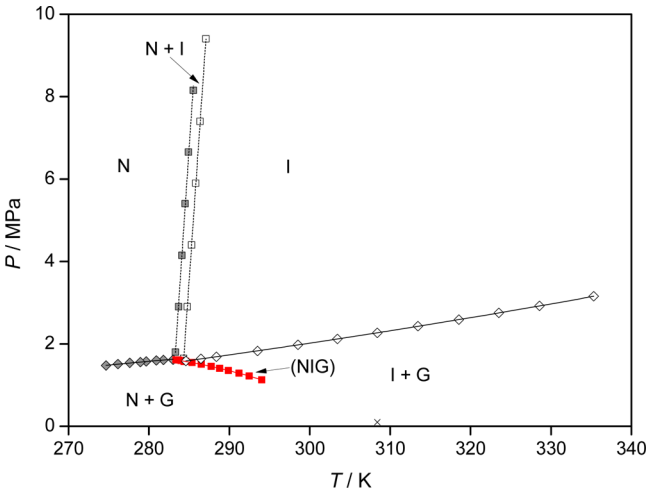

Figure 10. Metastable part of the *P,T* diagram of pentyl cyanobiphenyl + 5 mass % CO_2. Description of symbols used: (gray ■) N ↔ N + I, (□) N + I ↔ I, (gray ◆) N + G ↔ N, (◇) I + G ↔ I, (red ■) N + I + G, (×) N ↔ I phase transition for the pure LC at 1 bar. The three-phase curve is identified with a red line and symbols and has notation between parentheses.

dimers with benzene.[12] However, as the system is dense, the interaction between CO_2 and the benzene ring will also depend on, for example, the packing of the molecules and solvent−solvent interactions.

Assuming that the gas phase is pure CO_2 and the isotropic phase is an ideal mixture, the Henry coefficient, H, of CO_2 in the isotropic phase can be estimated using

$$H = \frac{f_{CO_2}}{x_{CO_2}} \quad (2)$$

Here, f_{CO_2} is the fugacity of pure CO_2 at the experimental bubble point pressure and x_{CO_2} is the CO_2 mole fraction in the isotropic liquid phase. Estimated Henry coefficients can be used to rank the CO_2 capacity of the solvents. Experimental bubble-point data from the experiments was used to calculate the Henry coefficients at 350 K using an equation of state for calculating the fugacity coefficient of CO_2; see Table 2.[13] In this table, it is shown that increasing the length of the hydrocarbon chain of the LC leads to a higher mole based solubility: PB and 8OCB have a lower mole based Henry coefficient than EP and 5OCB, respectively. For ionic liquids with different chain lengths, the same trend is observed.[11]

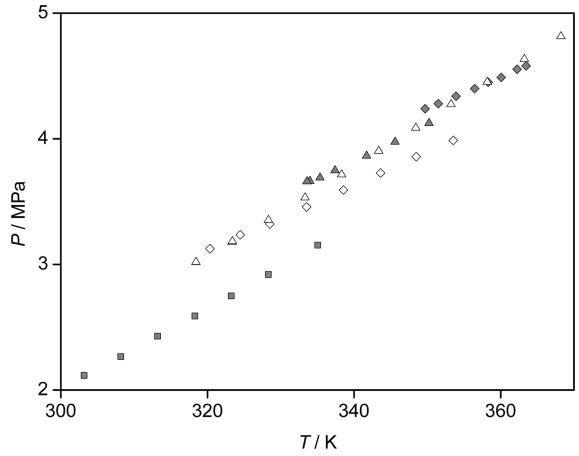

Figure 11. Bubble-point curves of various liquid crystals with 5 wt % CO_2. (gray ◆) propyl butyl bicyclohexyl, (◇) ethyl propyl bicyclohexyl, (gray ▲) octyloxy cyanobiphenyl, (△) pentyloxy cyanobiphenyl, (gray ■) pentylcyanobiphenyl.

Table 2. Estimated Henry Coefficients (H) for CO_2 in LCs at T = 350 K

	H (MPa)	
LC molecule	mole based	mass based
5CB	14.4	66.3
5OCB	15.3	73.5
8OCB	13.6	73.0
PB	15.5	74.2
EP	15.9	70.1

■ CONCLUSIONS

P,T phase diagrams have been determined for five liquid crystals with 5 mass % CO_2. Of the liquid crystals investigated, 5CB has the highest solubility of CO_2. The apolar liquid crystals tested, 3,4-BCH and 2,3-BCH, have the lowest solubility of CO_2. These liquid crystals are not suitable for CO_2 capture, because of the high viscosity of the smectic phase. 5OCB and 8OCB have a lower solubility of CO_2 than 5CB, probably caused by a distortion of the quadrupole moment of the benzene ring. The molar solubility of CO_2 was found to be higher for molecules with a longer hydrocarbon tail. The liquid crystals tested in this paper are not promising enough for a CO_2 capture process because of the low CO_2 solubility.

■ ASSOCIATED CONTENT

Supporting Information

Tables with *P,T* data of measured phase equilibria of LC with CO_2. This material is available free of charge via the Internet at http://pubs.acs.org.

dx.doi.org/10.1021/jp303426k | J. Phys. Chem. B 2012, 116, 9101−9106

AUTHOR INFORMATION

Corresponding Author

*Phone: +31-(0)15-278-6651. E-mail: t.w.deloos@tudelft.nl.

Notes

The authors declare no competing financial interest.

ACKNOWLEDGMENTS

Merck and Prof. Picken are acknowledged for providing free samples of liquid crystals. This research is supported by the Dutch Technology Foundation STW, applied science division of NWO and the Technology Program of the Ministry of Economic Affairs.

REFERENCES

(1) Pestov, S. Physical properties of liquid crystals. In *The Landolt-Börnstein database Group VIII: Advanced Materials and Technologies*; Vill, V., Ed.; Springer-Verlag: Berlin/Heidelberg, Germany, 2003; Vol. *5A*.

(2) Gross, J.; Jansens, P. J. Patent WO2008147181-A1; NL2000654-C2, 2008.

(3) de Loos, T. W.; van der Kooi, H. J.; Ott, P. L. *J. Chem. Eng. Data* **1986**, *31*, 166−168.

(4) de Loos, T. W. *J. Supercrit. Fluids* **2006**, *39*, 154−159.

(5) Lewis, G. N.; Randall, M. *Thermodynamics*, 2nd ed.; McGraw-Hill: 1961.

(6) Chen, D. S.; Hsiue, G. H. *Polymer* **1994**, *35*, 2808−2814.

(7) Chen, D. S.; Hsiue, G. H.; Schultze, J. D.; Song, B. H.; Springer, J. *Mol. Cryst. Liq. Cryst. Sci. Technol., Sect. A* **1993**, *237*, 85−95.

(8) Chen, G. H.; Springer, J. *Mol. Cryst. Liq. Cryst.* **2000**, *339*, 31−44.

(9) Hsiue, G. H.; Chen, D. S.; Hsieh, C. J. *Mol. Cryst. Liq. Cryst. Sci. Technol., Sect. A* **1994**, *241*, 187−193.

(10) de Groen, M.; Matsuda, H.; Vlugt, T. J. H.; de Loos, T. W. Manuscript in preparation.

(11) Muldoon, M. J.; Aki, S. N. V. K.; Anderson, J. L.; Dixon, J. K.; Brennecke, J. F. *J. Phys. Chem. B* **2007**, *111*, 9001−9009.

(12) Besnard, M.; Cabaco, M. I.; Talaga, D.; Danten, Y. *J. Chem. Phys.* **2008**, *129*, 224511.

(13) Span, R.; Wagner, W. *J. Phys. Chem. Ref. Data* **1996**, *25*, 1509−1596.

(14) Hulme, D. S.; Raynes, E. P. *J. Chem. Soc., Chem. Commun.* **1974**, 98−99.

(15) Oweimreen, G. A.; Morsey, M. A. *Thermochim. Acta* **2000**, *346*, 37−47.

(16) Orwoll, R. A.; Sullivan, V. J.; Campbell, G. C. *Mol. Cryst. Liq. Cryst.* **1987**, *149*, 121−140.

(17) Lai, L.-L.; Chen, J.-J.; Lin, Y.-G.; Lin, Y.-C.; Tzeng, W.-S.; Cheng, K.-L. *Liq. Cryst.* **2003**, *30*, 1449−1454.